


Article

Fault Mode Analysis and Convex Optimization-Based Fault-Tolerant Control for New Type Dissimilar Redundant Actuation System of Near Space Vehicle

Jian Huang¹, Jun Wang^{1,*}, Weikang Li¹, Di Liu² , Cun Shi² and Fan Zhang¹

¹ Beijing Institute of Automatic Control Equipment, Beijing 100120, China; huangjian421@126.com (J.H.); vaelwk@163.com (W.L.); rennai214@163.com (F.Z.)

² School of Automation Science and Electrical Engineering, Beihang University, Beijing 100191, China; liudi54834@buaa.edu.cn (D.L.); shicun@buaa.edu.cn (C.S.)

* Correspondence: dwill-wang@buaa.edu.cn

Abstract: A new type dissimilar redundant actuation system (NT-DRAS), which is composed of an electro-hydrostatic actuator (EHA) and an electro-mechanical actuator (EMA), is applied in high value unmanned aerial vehicles such as the future near space vehicles to improve their reliability and performance index simultaneously. Further improvement in the flight safety is achieved with the fault-tolerant control (FTC) technique which deals with system faults. This paper proposes a novel convex optimization-based fault-tolerant control (CO-FTC) strategy for the NT-DRAS subject to gradual faults which are included in the state space representation of the system. A convex analysis-based treatment for system uncertainty caused by gradual faults is applied to determine the control gain matrix. The existence condition of the control gain matrix is optimized in the linear matrix inequality (LMI) form. Finally, the determined subsystems based on the novel technique is used to solve the modeled robust FTC problem. Case studies of NT-DRAS subject to different gradual faults have been accomplished to illustrate the FTC necessity for NT-DRAS. Furthermore, the effectiveness of the proposed CO-FTC strategy is validated by comparative analysis of the simulation results.



Citation: Huang, J.; Wang, J.; Li, W.; Liu, D.; Shi, C.; Zhang, F. Fault Mode Analysis and Convex Optimization-Based Fault-Tolerant Control for New Type Dissimilar Redundant Actuation System of Near Space Vehicle. *Appl. Sci.* **2023**, *13*, 12567. <https://doi.org/10.3390/app132312567>

Academic Editor: Dario Richiedei

Received: 23 October 2023

Revised: 15 November 2023

Accepted: 17 November 2023

Published: 21 November 2023



Copyright: © 2023 by the authors. Licensee MDPI, Basel, Switzerland. This article is an open access article distributed under the terms and conditions of the Creative Commons Attribution (CC BY) license (<https://creativecommons.org/licenses/by/4.0/>).

Keywords: new type dissimilar redundant actuation system; near space vehicle; fault-tolerant control; linear matrix inequality

1. Introduction

The vehicle actuation system is an essential system used to realize vehicle trajectory control. The actuation system receives input from the flight control and drives the corresponding control surfaces to keep or adjust the attitude of the vehicle. In order to guarantee the vehicle safety and further enhance the reliability of a vehicle actuation system, a redundant system is commonly used for actuators and corresponding control surfaces. The common mode failure in a redundant actuation system, such as loss pressure fault due to physical damage or oil leakage in a redundant hydraulic actuation system, is a key factor limiting further enhancement of the system reliability. In order to solve this problem, the dissimilar redundant actuation system (DRAS) has attracted growing interest in industry and among researchers [1–4], due to its advantages of high reliability through avoidance of common mode failures. The most used DRAS is composed of a traditional hydraulic actuator (HA) and a new electro-hydrostatic actuator (EHA), which is usually used in large civil aircraft such as the A350 and A400M vehicles. However, for the vehicle with high power/weight ratio in the military domain such as an unmanned near space vehicle, the traditional DRAS no longer applies due to the heavy load of the hydraulic system. Considering the distributed flexible layout advantage of EHA and electro-mechanical actuator (EMA), this paper proposes a new type dissimilar redundant actuation system (NT-DRAS) composed of EHA and EMA for the near space vehicles. Meanwhile, to further improve the

reliability of NT-DRAS, fault-tolerant control (FTC) technique is used to minimize effects of possible faults and maintain the system performance at a desired level. There are two types of faults that can occur in NT-DRAS: sudden faults and gradual faults. The sudden faults typically lead to distinct system performance degradation, resulting in effective fault identification which can be used to address its side effects [5]. Alternately, gradual faults, such as oil leakage and flow changes, are difficult to detect and can gradually degrade the system performance and pose a problem that remains to be effectively solved.

FTC has evolved into two branches: passive fault-tolerant control (PFTC) and active fault-tolerant control (AFTC). Jiang and Yu [6] have conducted a comparative study of the two different approaches, and discovered that PFTC can be used to deal with the predicted faults while AFTC can be used to deal with unknown failures which may lead to catastrophic consequences. PFTC is typically adopted for designing fixed controllers with robustness against presumed faults and disturbance, and although it is of limited fault-tolerant capability, it does not require fault detection and control law reconfiguration. Niemann and Stoustrup [7] studied the PFTC problem of a double inverted pendulum. For comparison purposes and for the case of critical faults, they applied AFTC with active reconfiguration of the control law. They concluded that both PFTC and AFTC can maintain high stability and level of performance when the system suffers critical faults, but that AFTC requires real-time fault detection and diagnosis information. For example, Castaldi et al. [8] used AFTC in vehicle on the precondition of fault detection and diagnosis. Goupil studied the fault detection and isolation (FDI) and FTC problems in flight control system [9], and demonstrated the importance of FDI for the effectiveness of AFTC. For the complex and changing fault cases (including both minor and severe faults) of a system, PFTC and AFTC can be combined to develop comprehensive FTC strategies in different fault degree conditions [10]. Tao [11] presented a literature review emphasizing essentiality of the FDI process in the AFTC design. Consequently, the PFTC approach can be considered to be a better one when dealing with the reliability of FDI and the fault features in NT-DRAS systems with only gradual faults.

The robust control techniques are often used to address the FTC problem. For example, in order to maintain system performance under severe conditions such as actuator faults, robust control techniques can be used to develop a linear parameter varying (LPV) controller [12]. The efficiency of parameter identification with the robust control technique can be further improved with the adaptive technique [13], in which case the fault modes are modeled following the fault principles. For example, Tao et al. [14] modeled intermittent faults as Bernoulli distributed random variables and then designed a passive controller, while Zhang et al. [15] described the actuator failures as fuzzy discrete-time interconnected events. However, certain fault modes, such as the referred gradual faults in NT-DRAS, are difficult to detect because of no obvious fault characterization, and in those cases alternative fault modeling methods need to be considered.

The FTC with gradual faults and outside disturbance is considered to be equivalent to the problem of system robustness in this paper. Since the gradual faults in NT-DRAS present the uncertainty characteristics and are difficult to detect, gradual faults can be considered as system uncertainty [16]. The system uncertainty due to the gradual faults is different from the model uncertainty caused by the system identification error: The former one is caused by the changing gradual faults and can result in the system dynamic performance variant with adverse influences of different fault degree, while the latter one, under fault-free conditions, has only a minor adverse influence due to the invariant system parameter errors. The first type of uncertainty modeling method for system failures is also used in flight control systems, for example, Yu and Zhang [17] designed a passive fault tolerant controller against actuator failures. Tao [11] determined that system component failures are often treated as system uncertainties, and that the robust fault tolerant control can be used to deal with failure caused by the parameter variations and model uncertainties. Zhou and Zheng [18] studied a delayed singular system with linear fractional parameter uncertainty using robust control method. Wang et al. [19] analyzed the robust stability of stochastic delayed

genetic regulatory networks with polytope and linear fractional parameter uncertainties. In both of these latter two studies, all of the uncertainties are expressed in the form of uncertainty matrices, and are assumed to meet certain conditions. However, it is difficult to find matching conditions for NT-DRAS, and consequently application of the uncertainty modeling method in NT-DRAS requires some modifications. In Li and Yang's research [20], a robust fuzzy adaptive fault tolerant control method was proposed for a class of nonlinear systems with mismatched uncertainties and actuator faults. The research results indicate that the proposed method is effective for that particular class of nonlinear system with severe faults and mismatched uncertainties.

Application of a time-invariant controller is typically sufficient and effective in the case of systems with gradual faults. The controller provides the advantage of a simple control structure where the controller gains are commonly determined with linear matrix inequality (LMI) technique and a convex optimization. For example, the work by Chesi [21], who studied the LMI conditions for time-varying uncertain systems, indicates that LMI technique is effective for the uncertain systems. Kheloufi et al. [22] designed the observer-based controller for linear systems with parameter uncertainty. Liao et al. [23] studied the reliable robust flight tracking control using this technique. In the previously cited research, the LMI technique is used to realize the pole placement in order to form a stable closed-loop system and guarantee the system robustness. The major problem in the design of a fixed fault-tolerant controller by pole placement for NT-DRAS with gradual faults is to identify adequate representation of the system uncertainty and to determine the solution conditions using LMI technique.

In this paper, a novel convex optimization-based fault-tolerant control (CO-FTC) strategy is proposed for NT-DRAS subject to gradual faults. The gradual faults are included in the system's state space formulation according to the characteristics of the fault modes. The control gain matrix of the system with uncertainty is optimized by the convex analysis with solving conditions, which are determined from the subsystems in LMI form. As opposed to the existing optimization method, the proposed subsystem-based method can be used without matching conditions on the faults, providing a novel robust optimization treatment for the system with varying gradual faults and results in better system performance compared with traditional methods. The detailed work of this paper can be summarized as follows:

- (i) Typical gradual faults of NT-DRAS are included in the system's state space formulation in the form of uncertainty. In order to remove the system uncertainty, specific subsystems are obtained through convex analysis.
- (ii) A constant, time-invariant controller is designed based on LMI conditions, which are deduced from the subsystems of the original uncertain system. Compared with the traditional optimization method based on the original uncertain system, the proposed subsystem-based optimization technique can result in a more feasible time-invariant control gain under gradual fault conditions.
- (iii) The simulation analysis results are provided and observations are discussed. First, the effects of gradual faults on the system response performance in the time domain are analyzed based on the pole location. Second, comparative analysis is performed on the NT-DRAS under moderate fault conditions with the proposed controller and with the existing guaranteed cost controller.

This paper is organized as follows: Section 1 introduces the background of the proposed NT-DRAS and its FTC problem; Section 2 performs the system modeling under normal and fault conditions; Section 3 presents a novel model analysis and control gain optimization methodology; Section 4 gives the specific FTC structure design and control gain solving algorithm; Section 5 presents simulation analysis results; Section 6 gives conclusions and recommends the research content to be conducted in the future.

Notation: In this paper, Δ specifies parameter error, $\text{Re}\lambda_i(\cdot)$ is the form of eigenvalue real part, and $w(t) \in L_2[0, \infty)$ represents a quadratic differential function.

2. System Statement

The schematic structure of a NT-DRAS is composed of one EHA and one EMA (see Figure 1). As shown in Table 1, NT-DRAS can have three operating modes. Under the normal conditions, only EHA is used to drive the control surface while EMA is in the passive backup mode. In this operating mode, the chamber of EHA is separated into low-pressure (blue) and high-pressure (red) volumes, respectively, causing the piston to move. Meanwhile, EMA is pulled passively by the control surface actuated by EHA. Consequently, the EMA is considered to be in a no-load mode. This type of active/passive (A/P) operating mode, known as Mode-1, is the most common. Therefore, the convex optimization FTC strategy is developed for this operating mode, while Mode-2 is treated as an alternative one in the AFTC strategy [24]. Mode-3 occurs when the control surface actuated by the NT-DRAS requires a fast response in order to assist the vehicle to realize the attitude adjustment, or the control surface is under the high load conditions [25]. In these conditions, both EHA and EMA are required to jointly actuate the control surface.

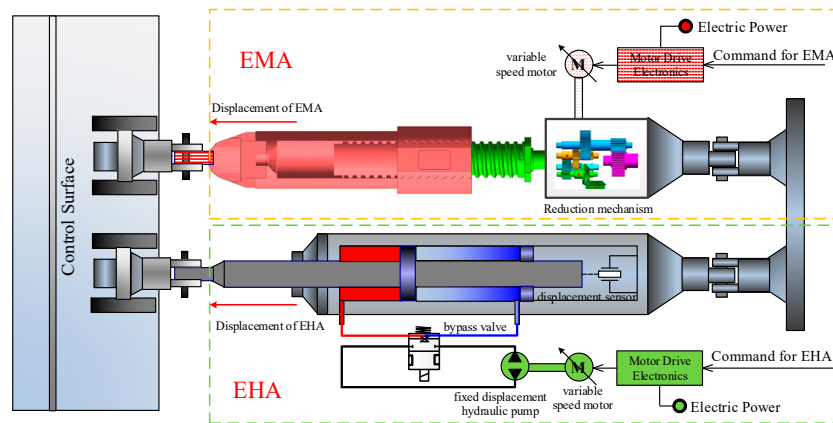


Figure 1. Schematic of proposed NT-DRAS in EHA_A/EMA_P mode.

Table 1. Operating modes of NT-DRAS.

Operating Modes	EHA Status	EMA Status	Working Condition
Mode-1: EHA _A /EMA _P	active	passive	normal
Mode-2: EHA _P /EMA _A	passive	active	EHA failed
Mode-3: EHA _A /EMA _A	active	active	high loaded

2.1. Modeling of Mode-1 in Normal Conditions

In Mode-1, EHA is the main working channel, with detailed modeling process given in this section. The main component and working principle is shown in Figure 2. It can be seen that in the motor pump section, the bidirectional piston pump, driven by the motor, connects directly to the motor.

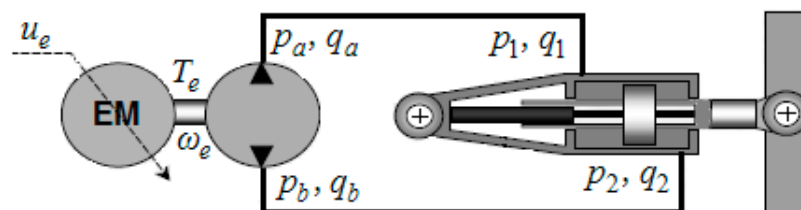


Figure 2. Component and schematic diagram of EHA channel.

2.1.1. Modeling of EHA Component

It is assumed that the brushless DC motor is used in this system. The motor armature and torque balance equations can be given as following, respectively:

$$\begin{cases} u_{\text{eha}} = C_e \omega_{\text{eha}} + L_e \frac{di_e}{dt} + R_e i_{\text{eha}} \\ K_m i_{\text{eha}} = T_{\text{eha}} + J_m \frac{d\omega_{\text{eha}}}{dt} + B_{me} \omega_{\text{eha}} \end{cases} \quad (1)$$

where u_{eha} , i_{eha} and ω_{eha} are the input voltage, output current and speed of the motor, respectively; C_e is the back EMF coefficient; K_m , L_e and R_e are the electromagnetic torque constant, inductance and resistance of the motor respectively; T_{eha} is the output torque of the motor; B_{me} is the simplified equivalent damping coefficient of the motor; J_m is the total moment of inertia of motor and pump.

In the pump-cylinder modeling link, the pump efficiency is assumed as 100%, and there is no pressure loss between the input and output of the cylinder, and the following pressure and flow equation can be given as:

$$\begin{cases} q_a = q_1, q_b = q_2 \\ p_a = p_1, p_b = p_2 \end{cases} \quad (2)$$

where p_1 and q_1 are the pressure and flow of the cylinder inlet, p_2 and q_2 are the pressure and flow of the cylinder outlet; p_a and q_a are the pressure and flow of the pump outlet, p_b and q_b are the pressure and flow of the pump inlet.

Since the motor output torque can be regarded as the pump input torque, and the pump efficiency is assumed as 100%, that means $q_a = q_b$, and the following torque balance equation can be given as:

$$T_{\text{eha}} = V_P (p_a - p_b) = V_P P_{\text{eha}} \quad (3)$$

where V_P is the pump output of EHA, P_{eha} is the cylinder pressure.

The equation relating the motor speed ω_{eha} to the system velocity \dot{x}_{eha} and the EHA cylinder pressure P_{eha} is given as:

$$V_P \omega_{\text{eha}} = A_{\text{eha}} \dot{x}_{\text{eha}} + \frac{V_{\text{eha}}}{4E_{\text{eha}}} \dot{P}_{\text{eha}} + C_{\text{ehal}} P_{\text{eha}} \quad (4)$$

where A_{eha} is area of EHA hydraulic cylinder; V_{eha} is volume of EHA hydraulic cylinder; E_{eha} is the volumetric modulus of elasticity; C_{ehal} is leakage coefficient of EHA hydraulic cylinder.

In the final output force link, the external load on the cylinder, F_{eha} , consists of three components: inertia and damping loads of EHA, inertia load of the control surface as well as EMA, and external disturbance, F_L , caused by gust, is given as:

$$A_{\text{eha}} P_{\text{eha}} = F_{\text{eha}} = (m_{\text{eha}} + m_{\text{ema}} + m_d) \ddot{x}_{\text{eha}} + (B_{\text{eha}} + B_{\text{ema}} + B_d) \dot{x}_{\text{eha}} + F_L \quad (5)$$

where B_{eha} , B_{ema} , and B_d are equivalent damping parameters of EHA hydraulic cylinder pistons, EMA transmission screw, and the control surface, respectively; m_{eha} , m_{ema} , m_d represent equivalent masses of EHA hydraulic cylinder piston, EMA transmission screw, and the control surface, respectively.

2.1.2. State Space Form of NT-DRAS in Mode-1

The state variables are defined as $x = [x_{\text{eha}}, \dot{x}_{\text{eha}}, P_{\text{eha}}, \omega_{\text{eha}}]^T$, by using the Equations (1)–(5), the state space representation of system can be derived as:

$$\begin{cases} \frac{dx_{\text{eha}}}{dt} = \dot{x}_{\text{eha}} \\ \frac{d\dot{x}_{\text{eha}}}{dt} = -\frac{B_{\text{eha}}+B_{\text{ema}}+B_{\text{d}}}{m_{\text{eha}}+m_{\text{ema}}+m_{\text{d}}}\dot{x}_{\text{eha}} + \frac{A_{\text{eha}}}{m_{\text{eha}}+m_{\text{ema}}+m_{\text{d}}}P_{\text{eha}} - \frac{1}{m_{\text{eha}}+m_{\text{ema}}+m_{\text{d}}}F_{\text{L}} \\ \frac{dP_{\text{eha}}}{dt} = -\frac{4E_{\text{eha}}A_{\text{eha}}}{V_{\text{eha}}}\dot{x}_{\text{eha}} - \frac{4E_{\text{eha}}C_{\text{ehal}}}{V_{\text{eha}}}P_{\text{eha}} + \frac{4E_{\text{eha}}V_{\text{P}}}{V_{\text{eha}}}\omega_{\text{eha}} \\ \frac{d\omega_{\text{eha}}}{dt} = -\frac{V_{\text{P}}}{J_{\text{m}}}P_{\text{eha}} - \frac{B_{\text{me}}}{J_{\text{m}}}\omega_{\text{eha}} + \frac{K_{\text{m}}}{J_{\text{m}}R_{\text{e}}}u_{\text{eha}} \end{cases} \quad (6)$$

In the state space form, Equation (6) can be represented as:

$$\begin{cases} \dot{x}(t) = Ax(t) + Bu(t) + Gw(t) \\ y(t) = Cx(t) \end{cases} \quad (7)$$

where $u(t)$ is the system input, $y(t)$ is the system output, $w(t) = F_{\text{L}}$ is unknown disturbance. The state, input, output, and disturbance matrices are presented in Equation (8).

$$\begin{cases} A = \begin{bmatrix} 0 & 1 & 0 & 0 \\ 0 & -\frac{B_{\text{eha}}+B_{\text{ema}}+B_{\text{d}}}{m_{\text{eha}}+m_{\text{ema}}+m_{\text{d}}} & \frac{A_{\text{eha}}}{m_{\text{eha}}+m_{\text{ema}}+m_{\text{d}}} & 0 \\ 0 & -\frac{4E_{\text{eha}}A_{\text{eha}}}{V_{\text{eha}}} & -\frac{4E_{\text{eha}}C_{\text{ehal}}}{V_{\text{eha}}} & \frac{4E_{\text{eha}}V_{\text{P}}}{V_{\text{eha}}} \\ 0 & 0 & -\frac{V_{\text{P}}}{J_{\text{m}}} & -\frac{B_{\text{me}}}{J_{\text{m}}} \end{bmatrix} \\ B = \begin{bmatrix} 0 & 0 & 0 & \frac{K_{\text{m}}}{J_{\text{m}}R_{\text{e}}} \end{bmatrix}^T \\ C = \begin{bmatrix} 1 & 0 & 0 & 0 \\ 0 & 1 & 0 & 0 \\ 0 & 0 & 1 & 0 \\ 0 & 0 & 0 & 1 \end{bmatrix} \\ G = \begin{bmatrix} 0 & -\frac{1}{m_{\text{eha}}+m_{\text{ema}}+m_{\text{d}}} & 0 & 0 \end{bmatrix}^T \end{cases} \quad (8)$$

An assumption is made that the above parameters are accurate standard values, so that there is no system uncertainty in the system model represented in Equation (7).

Remark 1. In the motor link modeling, the electromagnetic time constant can be represented as $T_1 = L_e/R_e$, the mechanical time constant can be represented as $T_2 = J_m/B_{me}$, since $T_1 \ll T_2$, and considering that the mechanical link is the dominant factor, the motor model can be simplified as a first-order process by ignoring the armature inductance and the back-EMF link:

$$\omega_{\text{eha}} = \frac{1}{J_{\text{m}}s + B_{\text{me}}} \left(\frac{K_{\text{m}}}{R_{\text{e}}}u_{\text{eha}} - T_{\text{eha}} \right) \quad (9)$$

2.2. Modeling of Mode-1 under Gradual Fault Conditions

2.2.1. System Component and Working Mode-Based Fault Analysis

In operating mode-1, which EHA is in active working mode while EMA is in passive working mode, EMA and the actuated control surface can be regarded as the load of EHA, therefore, B_{ema} and B_{d} can be seen constant; Similarly, the mass of EHA, EMA and the control surface stay consistent without physical damage, leading the three parameters m_{eha} , m_{ema} and m_{d} to be constant; As the component of EHA, the area and volume of EHA hydraulic cylinder also stay consistent without physical damage, leading the parameters A_{eha} and V_{eha} to be constant, the pump output V_{P} stay as constant since the pump structure is fixed designed. Without changing system structure and mass, the total moment of inertia of motor and pump J_{m} stay constant. In this paper, the electromagnetic torque constant K_{m} is also regarded as designed fixed constant. The rest system parameters C_{ehal} , B_{eha} ,

E_{eha} and R_e all have their own changing law caused by corresponding gradual fault types, which are introduced in the following section.

2.2.2. Gradual Fault Mechanism-Based System Model

The gradual faults of EHA can be classified in the above categories shown in Table 2, where the faults correspond with relative parameter drift: Fault-1 represents that leakage coefficient C_{ehal} changes due to the hydraulic cylinder leakage, Fault-2 represents that damping coefficient B_{eha} changes due to the increasing motion damping, Fault-3 represents that bulk modulus E_{eha} changes due to oil deteriorates caused by the air in oil, and Fault-4 represents that R_e changes due to its increasing caused by heat production. These types of gradual faults are difficult to detect and yet result in the system performance degradation. The relative parameters drift with the gradual fault degrees within limited ranges. Though similar to the system model uncertainty in fault-free conditions, the gradual faults cause more severe parameter drift, which can be regarded as gradual faults caused by the system uncertainty. In order to model these faults in NT-DRAS, uncertainty matrices are used to describe the parameter uncertainty caused by these faults. The NT-DRAS model of the mode-1 with gradual faults can be represented in state-space form as:

$$\begin{cases} \dot{x}(t) = (A + \Delta A)x(t) + (B + \Delta B)u(t) + Gw(t) \\ y(t) = Cx(t) \end{cases} \quad (10)$$

where ΔA and ΔB are deviations in the original state and input matrices caused by parameter changes due to the gradual faults. It is necessary to state that the gradual faults caused deviation matrices have more adverse effect compared with the system model uncertainty under fault-free conditions. There is no ΔC in the above system description, as it is assumed that all of the sensors are operating normally. The system matrices and the fault module matrices can be expressed as:

$$\begin{cases} A = \begin{bmatrix} 0 & 1 & 0 & 0 \\ 0 & a_{22} & a_{23} & 0 \\ 0 & a_{32} & a_{33} & a_{34} \\ 0 & 0 & a_{43} & a_{44} \end{bmatrix} \\ B = [0 \ 0 \ 0 \ b_{41}]^T \\ \Delta A = \begin{bmatrix} 0 & 0 & 0 & 0 \\ 0 & \Delta a_{22} & 0 & 0 \\ 0 & \Delta a_{32} & \Delta a_{33} & \Delta a_{34} \\ 0 & 0 & 0 & 0 \end{bmatrix} \\ \Delta B = [0 \ 0 \ 0 \ \Delta b_{41}]^T \end{cases} \quad (11)$$

where coefficients of the state and input matrices, A and B , are defined in Equation (8); $\Delta a_{22} = -\Delta B_{\text{eha}} / (m_{\text{eha}} + m_{\text{ema}} + m_d)$ represents damping fault induced factor; $\Delta a_{32} = -4\Delta E_{\text{eha}} A_{\text{eha}} / V_{\text{eha}}$ is the bulk modulus fault factor; $\Delta a_{33} = -[4(\Delta E_{\text{eha}}) \cdot (\Delta C_{\text{ehal}})] / V_{\text{eha}}$ represents the bulk modulus as well as the internal leakage fault factor; $\Delta a_{34} = 4\Delta E_{\text{eha}} V_P / V_{\text{eha}}$ represents the bulk modulus fault factor; $\Delta b_{41} = K_m / (J_m \Delta R_e)$ represents the motor armature resistance fault factor. After making the following definitions $A_F = A + \Delta A$ and $B_F = B + \Delta B$, the model of NT-DRAS in Mode-1 can be described as a system with uncertainty in the following form:

$$\begin{cases} \dot{x}(t) = A_F x(t) + B_F u(t) + Gw(t) \\ y(t) = Cx(t) \end{cases} \quad (12)$$

Table 2. Fault types and corresponding coefficient.

Number	Illustration	The Corresponding Coefficient
Fault-1	Hydraulic cylinder leakage	leakage coefficient C_{eha}
Fault-2	Motion damping increasing	damping coefficient B_{eha}
Fault-3	Oil deterioration	bulk modulus E_{eha}
Fault-4	Resistance increasing	motor armature resistance R_e

3. Analysis of Fault Model by Using Convex Optimization

The gradual faults have more adverse effects on the system performance compared with the system uncertainty in fault-free conditions. The parameter drift due to the faults is difficult to identify in a timely manner due to the lack of matching conditions when designing the controller. Therefore, the existing treatment method of system uncertainty would not be feasible for the issue discussed in this paper. In order to solve the FTC problem with system gradual faults, new fault modeling method and FTC gain optimization techniques are applied in this paper.

3.1. Treatment of the Fault Model Uncertainty

Since this work considers only the gradual faults in NT-DRAS, it is reasonable to assume that the fault signature in parameter drift form is limited. Hence, upper bounds $|\Delta A|_{\text{bound}}$ and $|\Delta B|_{\text{bound}}$ for the uncertainty matrices ΔA and ΔB can be defined. To describe the system with uncertainty using defined upper bounds, two other time independent factors ρ_A and ρ_B are introduced, both of which are random variables from the interval $[-1, +1]$. Finally, another form of the original system with gradual faults can be obtained as:

$$\begin{cases} \dot{x}(t) = (A + \rho_A |\Delta A|_{\text{bound}})x(t) + (B + \rho_B |\Delta B|_{\text{bound}})u(t) + Gw(t) \\ y(t) = Cx(t) \end{cases} \quad (13)$$

where

$$\begin{cases} |\Delta A|_{\text{bound}} = \begin{bmatrix} 0 & 0 & 0 & 0 \\ 0 & |\Delta a_{22}|_{\text{bound}} & 0 & 0 \\ 0 & |\Delta a_{32}|_{\text{bound}} & |\Delta a_{33}|_{\text{bound}} & |\Delta a_{34}|_{\text{bound}} \\ 0 & 0 & 0 & 0 \end{bmatrix} \\ |\Delta B|_{\text{bound}} = \begin{bmatrix} 0 \\ 0 \\ 0 \\ |\Delta b_{41}|_{\text{bound}} \end{bmatrix} \end{cases} \quad (14)$$

To form a closed-loop system, the state feedback $K_x x(t)$ was usually chosen as a part of the system input $u(t)$, where K_x is state feedback control gain. Since gradual faults can affect the pole position, and assuming that the gradual faults are limited, the following assumption is made as a basis of proof and following conclusions.

Assumption 1. *The gradual faults are assumed to be limited and their effects on the system can be expressed in the form of the closed-loop system eigenvalues, where the real parts of the eigenvalues of the fault system change according to the following inequality relationship with respect to the fault-free system*

$$\begin{cases} |\text{Re}\lambda_i(|\Delta A|_{\text{bound}})| < |\text{Re}\lambda_i(A)| \\ |\text{Re}\lambda_i(|\Delta B|_{\text{bound}} K_x)| < |\text{Re}\lambda_i(BK_x)| \end{cases} \quad (15)$$

In order to determine the controller gains, based on the upper bounds of the uncertainty matrices, the deterministic model needs to be obtained. Here, the extremums of

ρ_A and ρ_B are considered, resulting in four critical subsystems as the boundary condition models to be used by the LMI technique.

$$\begin{cases} \dot{x}(t) = (A \pm |\Delta A|_{\text{bound}})x(t) + (B \pm |\Delta B|_{\text{bound}})u(t) + Gw(t) \\ y(t) = Cx(t) \end{cases} \quad (16)$$

The following section discusses the relationship between the original system with uncertainty and its four critical subsystems (see Equation (16)).

3.2. Rationality Analysis of Solving Conditions Using Convex Optimization

Since the control gain matrix is regarded as the solution of convex optimization using LMI technique, therefore, the optimization condition needs to be determined such that the optimized solution results in the stable system.

To obtain the solving conditions for the control law, the four critical subsystems are chosen as the controlled plants instead of the original system with uncertainty. Based on these four specific subsystems, the premise of optimization is determined and then the solution is obtained using the LMI technique. The FTC law existence condition using this treatment is at least sufficient, which is stated in Lemma 1.

There are four stable areas of the subsystems under an assumed feedback (see Figure 3). According to the convex optimization, the optimized stable area of the closed-loop system will be located at the intersection of the four areas. This corresponds to LMI technique approach to determine the control gain matrix. In this instance there are four LMIs due to the multiple solving conditions, which is similar to the conditions presented in [26], where Huang et al. studied the LPV tracking problem using multiple Lyapunov functions. Although the solving condition is critical, since the stability region becomes smaller, the optimized solution will be at least sufficient once its existence is established. The method proposed in this paper deals with the problem of determining control gains for systems with uncertainty.

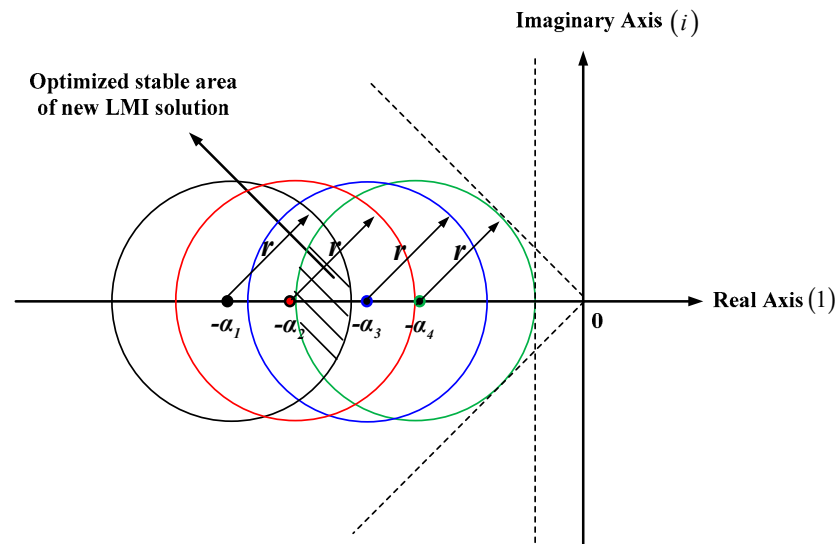


Figure 3. Optimized stable area of the closed-loop system using convex optimization.

Lemma 1. If a state feedback control gain matrix K_x can result in a stable system matrix $A_L + B_L K_x$, then it also results in a stable uncertain controllable matrix pair $(A + \Delta A \quad B + \Delta B)$, where

$$\begin{cases} A_L \in \{ A + |\Delta A|_{\text{bound}}, A - |\Delta A|_{\text{bound}} \} \\ B_L \in \{ B + |\Delta B|_{\text{bound}}, B - |\Delta B|_{\text{bound}} \} \end{cases} \quad (17)$$

in which, $A_L \in \{A + |\Delta A|_{\text{bound}}, A - |\Delta A|_{\text{bound}}\}$ means that the matrix A_L can be chosen as $A + |\Delta A|_{\text{bound}}$ or $A - |\Delta A|_{\text{bound}}$, which represent the system's upper and lower bound matrices due to gradual faults. Similarly, $B_L \in \{B + |\Delta B|_{\text{bound}}, B - |\Delta B|_{\text{bound}}\}$ means that the matrix B_L can be determined as $B + |\Delta B|_{\text{bound}}$ or $B - |\Delta B|_{\text{bound}}$, which represent the control upper and lower bound matrices due to gradual faults.

Proof of Lemma 1. See Appendix A. \square

4. FTC Structure and Controller Design for NT-DRAS

4.1. FTC Structure for All Fault Process

Since the proposed NT-DRAS may be subject to all faults including gradual types and sudden types, the whole FTC structure for all fault processes is given in Figure 4. In the structure, there are PFTC controllers, AFTC controllers and controller switching mechanisms for NT-DRAS. The switching law is designed based on the output result of the FDD scheme and a performance evaluation mechanism is first designed to provide quantitative results for FDD scheme. The index of the following performance evaluation criterion in Euclid norm form is given as:

$$e_{\text{perf}}(t) = \|r(t) - y(t)\|_2 \tag{18}$$

where $r(t)$ is the reference signal, while $y(t)$ is the NT-DRAS output. In order to measure the conservatism of the NT-DRAS under different fault conditions, also when used as FTC strategies, the mean and maximum value of $e_{\text{perf}}(t)$, $t \in [t_1, t_2]$, are also defined in the following forms and used as the overall performance measures.

$$\left\{ \begin{aligned} \bar{e}_{\text{perf}}(t) &= \frac{1}{t_2 - t_1} \int_{t_1}^{t_2} e_{\text{perf}}(t) dt \\ e_{\text{perf-max}} &= \max\{e_{\text{perf}}(t), t \in [t_1, t_2]\} \end{aligned} \right\} \tag{19}$$

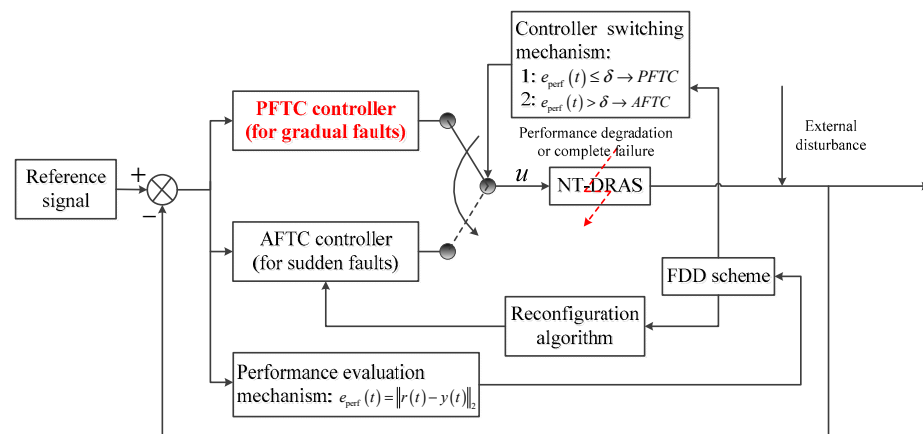


Figure 4. FTC structure for all fault processes.

A preset tracking performance value δ is also given as a threshold, which is used to determine whether to switch the PFTC controller. When $e_{\text{perf}}(t) \leq \delta$, it means the PFTC controller is still effective for the gradual fault conditions, once $e_{\text{perf}}(t) > \delta$, AFTC controller should be enabled to maintain the NT-DRAS performance under severe fault conditions. This paper is dedicated to the PFTC controller design and the AFTC strategy design for severe faults is listed as future research work.

4.2. Controller Design for NT-DRAS Subjected to Gradual Faults

The FTC problem considered in this paper is to design a controller for NT-DRAS with gradual faults, similar to the ones discussed in [23,27], such that

1. Under the gradual fault conditions, the NT-DRAS output $S_{out}y(t)$ tracks the reference signal $r(t)$ without steady-state error, that is $\lim_{t \rightarrow \infty} e(t) = 0$, where $e(t) = r(t) - S_{out}y(t)$, $S_{out} = [1 \ 0 \ 0 \ 0]$
2. The optimized performance to be defined later can be achieved by the designed controller. The corresponding augmented system can be described in the following form.

$$\begin{cases} \dot{x}_{aug}(t) = A_{aug}x_{aug}(t) + B_{aug}u(t) + G_{aug}w_{aug}(t) \\ y_{aug}(t) = C_{aug}x_{aug}(t) \end{cases} \quad (20)$$

where $x_{aug}(t) = [\int e(t)dt \ x(t)]^T$ is the augmented state vector, $y_{aug}(t) = [\int e(t)dt \ y(t)]^T$ is the augmented output vector, $w_{aug}(t) = [r(t) \ w(t)]^T$ is the augmented disturbance vector, and the corresponding augmented matrices are as follows $A_{aug} = \begin{bmatrix} 0 & -S_{out}C \\ 0 & A_F \end{bmatrix}$, $B_{aug} = \begin{bmatrix} 0 \\ B_F \end{bmatrix}$, $C_{aug} = \begin{bmatrix} I & 0 \\ 0 & C \end{bmatrix}$, and $G_{aug} = \begin{bmatrix} I & 0 \\ 0 & G \end{bmatrix}$. The output feedback method is used to design a fault-tolerant controller when it is sufficient to realize some but not all control performance factors [28,29]. The closed-loop controller is designed using state and output error integration feedback form as follows, which is essentially a PI controller:

$$u(t) = Kx_{aug}(t) = K_e \int_0^t e(\tau)d\tau + K_x x(t) \quad (21)$$

where $K = [K_e \ K_x]$ is the fixed gain matrix to be solved by the LMI technique.

Define the linear-quadratic (LQ) cost function as

$$J = \int_0^t (x_{aug}^T(\tau)Qx_{aug}(\tau) + u(\tau)^TRu(\tau))d\tau \quad (22)$$

where Q and R are symmetric positive semi-definite and positive definite weighting matrices, respectively. Then the optimization objective is to design the control input form (see Equation (21)), so as to minimize the cost function. The following lemmas are introduced before the control gain matrix theorem is presented in further text.

Lemma 2 (Bounded Real Lemma). For the linear system form derived from Equation (16), and represented in the following form

$$\begin{cases} \dot{x}(t) = (A_L + B_L K_x)x(t) + Gw(t) \\ y(t) = Cx(t) \end{cases} \quad (23)$$

the transfer function form $G(s) = C(sI - A_L - B_L K_x)$ can be obtained. For a given performance index $\gamma : \|y(t)\| \leq \gamma \|w(t)\|$, if a real matrix $P = P^T > 0$ exists and satisfies the following matrix inequality

$$\begin{bmatrix} (A_L + B_L K_x)P + P(A_L + B_L K_x)^T & I & (CP)^T \\ * & -\gamma^2 I & I \\ * & * & -I \end{bmatrix} < 0 \quad (24)$$

then the system form represented by Equation (16) is stable and the transfer function $G(s)$ satisfies $\max\{\|G(s)\|\} < \gamma$.

Remark 2. The parameter γ represents the robust performance of the system and describes the quantitative relationship between the disturbance w and the system output y . The inequality $\max\{\|G(s)\|\} < \gamma$ means that the influence of the disturbance w on the system output y is limited in the gain level γ [30].

Lemma 3 (Reciprocal Projection Lemma) [31]. Let P be any given positive definite matrix. The following statements are equivalent:

1. $\psi + \zeta + \zeta^T < 0$;
2. The LMI problem
$$\begin{bmatrix} \psi + P - (S + S^T) & \zeta^T + S^T \\ \zeta + S & -P \end{bmatrix} < 0$$
 is feasible with respect to S , where ψ and ζ are a symmetric matrix and a general matrix, respectively.

Lemma 4 (Schur Complement Lemma) [32]. For the given symmetric matrix $S = \begin{bmatrix} S_{11} & S_{12} \\ S_{12}^T & S_{22} \end{bmatrix}$, the following three statements are equivalent:

1. $S < 0$;
2. $S_{11} < 0, S_{22} - S_{12}^T S_{11}^{-1} S_{12} < 0$;
3. $S_{22} < 0, S_{11} - S_{12} S_{22}^{-1} S_{12}^T < 0$.

The considered fault-tolerant controller with fixed structure and external disturbance, is in the state and output error integration feedback form (see Figure 5), realizing the pole placement and guaranteeing the robust performance. In order to solve for the controller gain, the determinate fault degree bounds and the anti-disturbance level are chosen for the proposed LMI algorithm. The existence conditions of the fault-tolerant controller gain are given in the form of the following theorem.

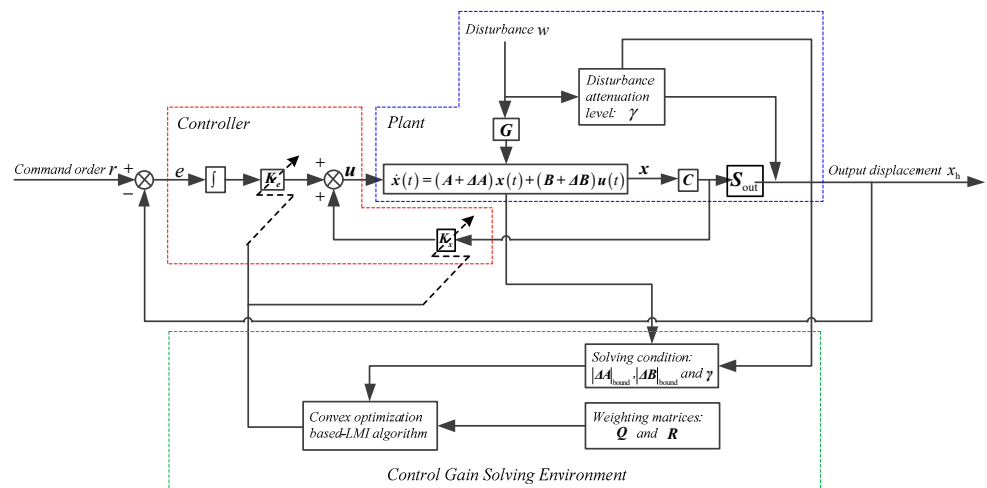


Figure 5. Controller structure for system with gradual faults in uncertain form.

Theorem 1. Consider the closed-loop augmented system with uncertainty (see Equation (20)). For a given scalar $\gamma > 0$ in Lemma 2, and for all nonzero disturbance inputs $w(t) \in L_2[0, \infty)$, choose Q and R as weighting matrices of linear quadratic (LQ) index, and define a symmetric positive definite matrix $P = X^{-1}$, and other appropriately dimensioned common matrices V, N and G . If these matrices can make the LMI conditions (see (A12)) hold, where in (A12), $A_{augL} = \begin{bmatrix} 0 & -S_{out}C \\ 0 & A_L \end{bmatrix}$, $B_{augL} = \begin{bmatrix} 0 \\ B_L \end{bmatrix}$, then the closed-loop system with uncertainty (see Equation (20)) can obtain the upper bound for performance indices in the following form

$$J < x_{aug}^T(0)Px_{aug}(0) + \gamma^2 \int_0^t w_{aug}^T(\tau)w_{aug}(\tau)d\tau \tag{25}$$

The control gain matrix of the fault-tolerant controller for the closed-loop system can be determined as $K = N_{\text{optimal}} V_{\text{optimal}}^{-1}$ where N_{optimal} and V_{optimal} are the optimal solutions to the four LMIs (see (A12)).

Proof of Theorem 1. See Appendix B. \square

5. Simulation Analysis

5.1. System Parameters for Fault Scenarios

5.1.1. Coefficient Setting and System Performance Analysis

To illustrate the necessity of the FTC, a NT-DRAS with different gradual fault scenarios (single fault conditions and all faults in combination ones) is used for simulation study and analysis, where the system parameters are the same as in [25]. Then the system matrices in normal conditions can be determined. Typical gradual faults of EHA have been discussed in Section 2.2. Since these gradual faults are considered to be of limited range and for design of the baseline robust time-invariant fault-tolerant controller, different matrices changing bounds need to be determined. The variation ranges of the relative parameters are chosen based on their standard values and the rationality can be verified by using pole analysis method as shown in Table 3.

Table 3. Parameter variation ranges.

Fault Types	Variation Ranges of the Relative Parameters
Fault-1	$C_{\text{ehal}} : 0.1 \times 10^{-10} \rightarrow 1.0 \times 10^{-10} \text{ [(m}^3\text{/s)/Pa]}$
Fault-2	$B_{\text{eha}} : 1.0 \times 10^4 \rightarrow 1.0 \times 10^5 \text{ [Ns/m]}$
Fault-3	$E_{\text{eha}} : 8.0 \times 10^8 \rightarrow 5.0 \times 10^8 \rightarrow 8.0 \times 10^7 \text{ [Pa]}$
Fault-4	$R_e : 0.245 \rightarrow 0.275 \text{ [\Omega]}$

As the upper bound of the gradual faults increases, pole positions under different fault conditions demonstrate tendency of moving towards imaginary axis (see Figure 6a), indicating that the system response is degraded by the gradual faults. Also, the circles indicate pole distribution areas under different fault conditions, thus demonstrating a tendency for convergence. It is necessary to point out that under the fault conditions, not only that the poles move towards the imaginary axis, but some of them are also moving away from the real axis, resulting in oscillatory system response. There is relationship between pole locations and the severity of the system fault (see Figure 6b). The dominant poles corresponding to system fault are obtained by the dominant pole analysis method. The third and fourth ones are taken as the dominant poles due to the relationship between the pole position and the system performance. The results are shown in Figure 6b, where arrows in the horizontal direction show the increase in the system fault, and the vertical arrows show the corresponding change in the position of the closed-loop poles. The four subfigures indicate that the dominant poles move towards the imaginary axis as the fault increases. In this process, the changing trajectory of E_{eha} coefficient relevant dominant pole exhibits nonlinear characteristics, an inflection point occurs in the vicinity of value 5.0×10^8 , and system performance before and after the inflection point should be analyzed and simulated.

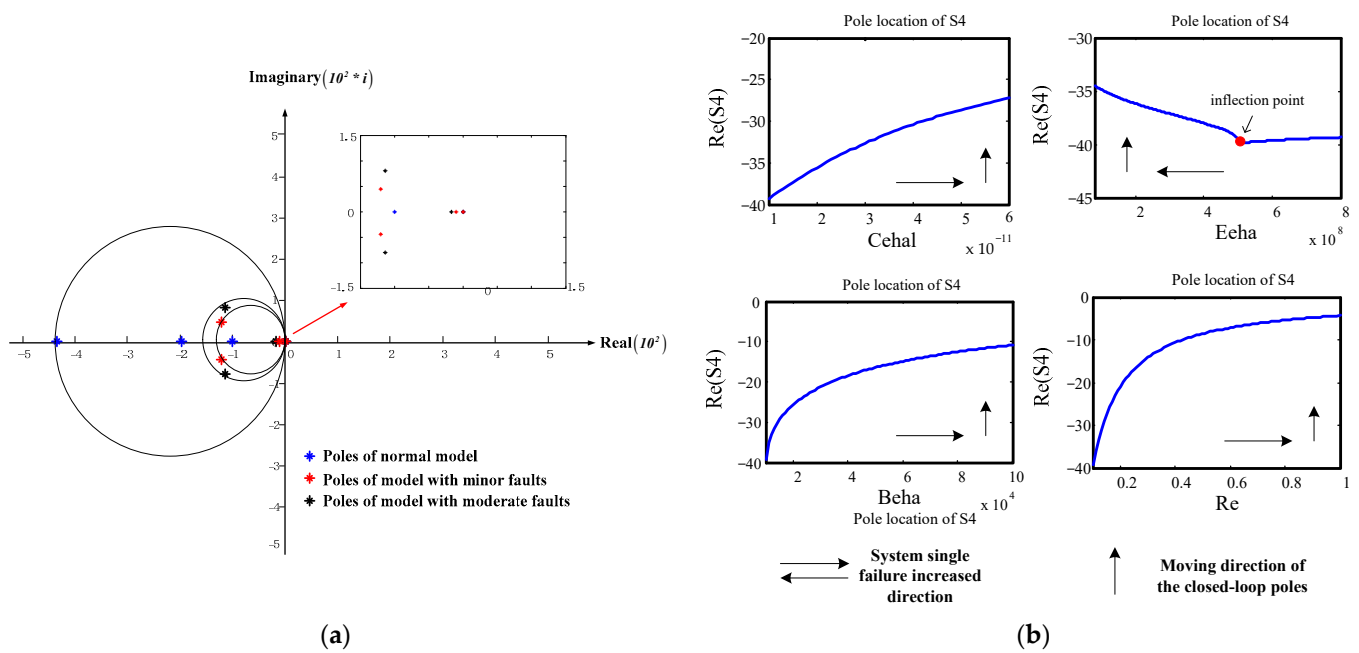


Figure 6. Pole position analysis for the open-loop system: (a) Pole positions in different conditions; (b) Relationship between pole position and system single fault.

5.1.2. Single Fault Effect Analysis under Closed-Loop System Conditions

It can be seen from Figure 6b that, the changing law of Fault-1, Fault-3 and Fault-4, shows consistency, while the changing law of Fault-2 shows nonlinear characteristics with an obvious inflection point. Therefore, two sets of simulation results, before and after the inflection point are performed.

By using the performance evaluation algorithm shown in Equations (18) and (19), to calculate the quantized value, the start and end times are set as $t_1 = 0$ and $t_2 = 8$, all evaluation results are shown in Table 4. The increasing of the $e_{perf}(t)$ value indicates the gradual fault effectiveness of the system performance degradation. It can be figured out that the oil leakage of the cylinder is a fault type with the greatest impact.

Table 4. System performance evaluation values under different single fault conditions without FTC (before the inflection point of fault-3 pole position trajectory).

Fault Types	$e_{perf}(t)$	$\bar{e}_{perf}(t)$	$e_{perf-max}$
Normal	0.2723	0.0001429	0.03
Fault-1	0.3631	0.0002581	0.03
Fault-2	0.3142	0.0001954	0.03
Fault-3	0.2728	0.0001432	0.03
Fault-4	0.2865	0.0001598	0.03

Only the final output displacement is used to evaluate the tracking performance here.

The system state response when only a single fault occurs is given in Figure 7. Compared with the normal state, among the four fault modes, the Fault-1 can have the greatest effect on the system performance (see Figure 7a): Under this type fault condition, in order to track the given step signal command order, even as the motor speed reaches its maximum value (see Figure 7d), the cylinder pressure can only reach a low level (see Figure 7c), leading the system output velocity to slow down to the slowest degree (see Figure 7b); The Fault-2 can have a secondary effect on the system performance (see Figure 7a): in order to track the given step signal command order, the motor speed also reaches a high level (see Figure 7d); however, since the motion damping increases, the cylinder pressure reaches the highest level due to the reverse motion damping caused force (see Figure 7c),

but can only have a faster system output velocity (see Figure 7b); The Fault-4 can also have obvious effect on the system performance (see Figure 7a): the EHA motor resistance increases due to heat production caused high temperature, leading to the motor speed decreasing significantly (see Figure 7d), and the cylinder pressure and the system output velocity also decrease eventually (see Figure 7b,c); The Fault-3 have the minimal effect on the system performance (see Figure 7a): Figure 7a,b,d show that the system output state almost have the same performance level as the system under normal state conditions. However, the cylinder pressure is at a low level due to the bulk modulus changes caused by oil deterioration (see Figure 7c).

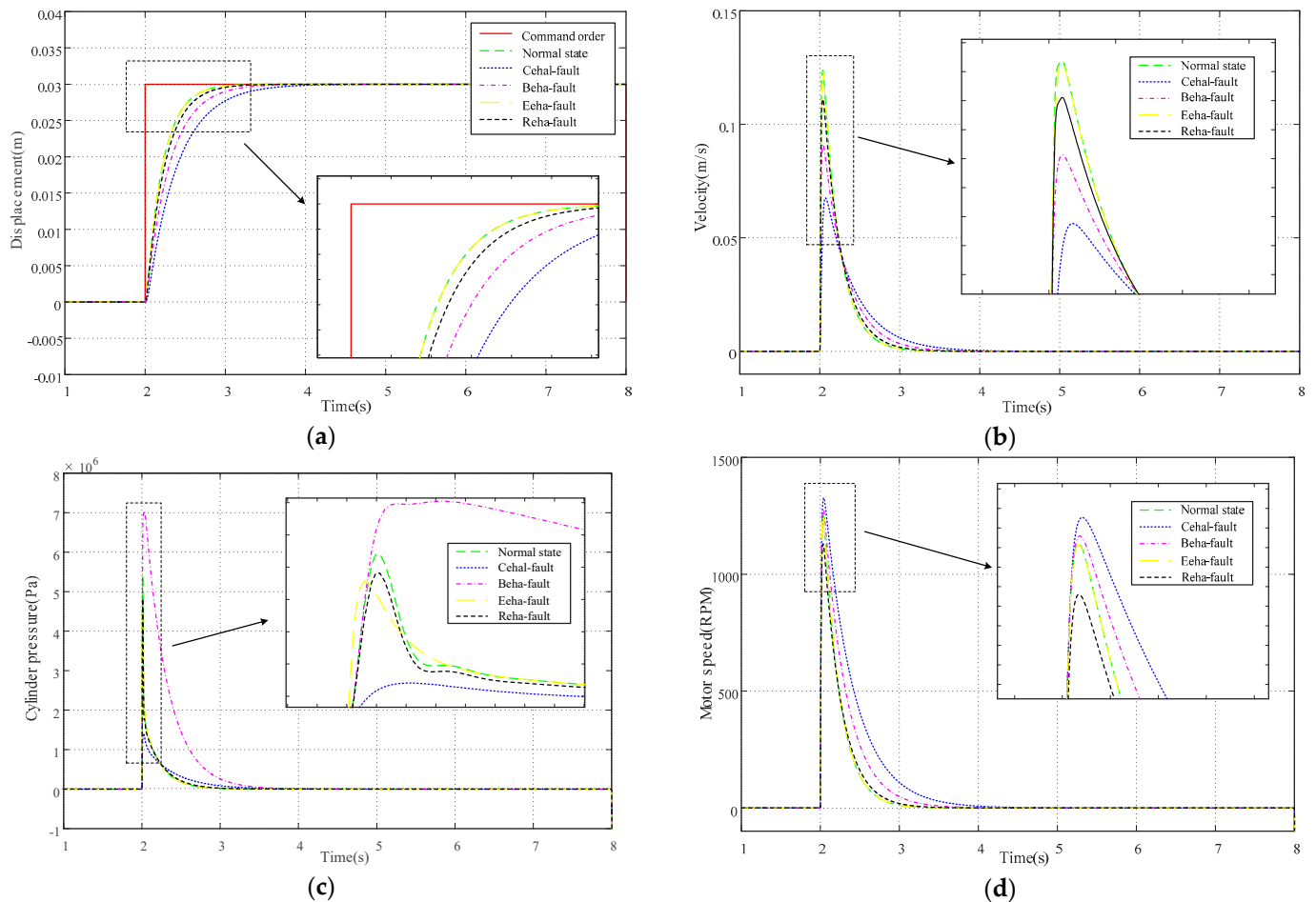


Figure 7. System state response under single fault conditions (before the inflection point of S4 location trajectory): (a) System displacement response; (b) System output velocity response; (c) System cylinder pressure response; (d) Motor speed response.

To analyze the nonlinear characteristic of the Fault-3 effect, another set of simulation results is shown in Figure 8 with the evaluation results in Table 5, in which the remaining fault modes (Fault-1, 2 and 4) are set as the same with the first simulation scenarios. When the Fault-3 dominant pole position across the inflection point, leading the bulk modulus value to the lowest level, the motor speed and the final system displacement output have slight performance degradation compared with the system under normal state (see Figure 8a,d and Table 5, in which the $e_{\text{perf}}(t)$ value changed to 0.2757 compared with the original 0.2728 in Table 4). However, the cylinder pressure is at a relatively low level with obvious fluctuations, and the system output velocity is significantly higher than the normal state with also obvious fluctuations.

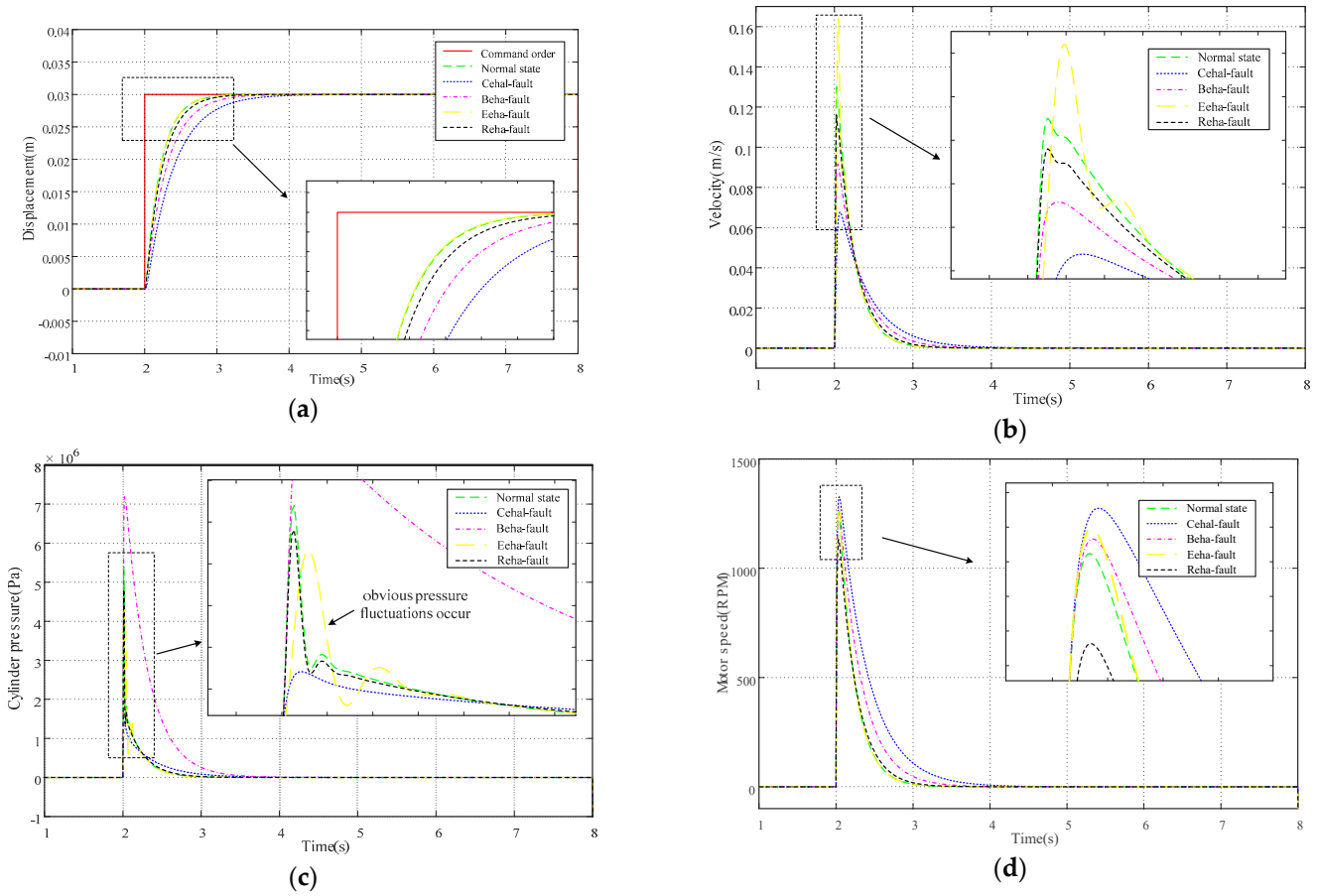


Figure 8. System state response under single fault conditions (after the inflection point of S4 location trajectory): (a) System displacement response; (b) System output velocity response; (c) System cylinder pressure response; (d) Motor speed response.

Table 5. System performance evaluation values under different single fault conditions without FTC (after the inflection point of fault-3 pole position trajectory).

Fault Types	$e_{\text{perf}}(t)$	$\bar{e}_{\text{perf}}(t)$	$e_{\text{perf-max}}$
Normal	0.2723	0.0001429	0.03
Fault-1	0.3631	0.0002581	0.03
Fault-2	0.3142	0.0001954	0.03
Fault-3	0.2757	0.0001432	0.03
Fault-4	0.2865	0.0001598	0.03

Only the final output displacement is used to evaluate the tracking performance here.

The two dominant closed-loop poles symmetrically distributed can be used to define the system performance range. First, define the largest interval matrix of the performance degradation due to the gradual faults as $\psi_{\text{max}} = \text{diag} \left[\frac{\text{Re}(\bar{S}_3)}{\text{Re}(S_3)}, \frac{\text{Re}(\bar{S}_4)}{\text{Re}(S_4)} \right]$, where \bar{S}_3, \bar{S}_4 are the dominant closed-loop poles of the system under the Mode-2 (EHA_P/EMA_A) operating mode. Then, divide the largest interval matrix of performance degradation into $(m - 1)$ intervals to form m system performance status. The first interval matrix represents the system performance under normal conditions, which can be described as $\psi_1 = \text{diag}[1, 1]$. Therefore, the $(k - 1)$ interval degradation matrix corresponding to the $(k - 1)$ level degree of fault is $\psi_k = \text{diag}[\psi_{k3}, \psi_{k4}]^T = \psi_1 - (k - 1) \frac{(\psi_1 - \psi_{\text{max}})}{m - 1}$, $k = 1, \dots, m$. Integrating the $(k - 1)$ th eigenvalues, the system matrix under the relative fault condition can be obtained as $\Lambda_k = \psi_k \Lambda_1, k = 1, \dots, m$. Then the transfer function and the corresponding state space

form system with different gradual faults level can be obtained. In this paper, the largest interval matrix is divided into three intervals, resulting in the four system performance status: (a) system in normal conditions, (b) system with minor fault conditions, (c) system with moderate fault conditions, and (d) system with major fault conditions, respectively. Using the above fault level determination principle, the system matrices changing bounds for the minor fault and moderate fault can be calculated and shown in the last two rows of Table 6.

Table 6. NT-DRAS system parameters with different fault upper bound scenarios.

Fault Degree	System Status	System Matrices	Control Matrices
Degree-1	Normal system	$A = \begin{bmatrix} 0 & 1 & 0 & 0 \\ 0 & -31.408 & 2.0704 \times 10^{-6} & 0 \\ 0 & -3.20 \times 10^{10} & -5.9864 \times 10^2 & 5.8776 \times 10^{13} \\ 0 & 0 & -9.9472 \times 10^{-5} & -1.0 \times 10^2 \end{bmatrix}$	$B = \begin{bmatrix} 0 \\ 0 \\ 0 \\ 456.63 \end{bmatrix}$
Degree-2	Minor failure	$ \Delta A _{\text{bound}}^1 = \begin{bmatrix} 0 & 0 & 0 & 0 \\ 0 & 28.169 & 0 & 0 \\ 0 & 0.11 \times 10^{10} & 1.7959 \times 10^2 & 1.7633 \times 10^{13} \\ 0 & 0 & 0 & 0 \end{bmatrix}$	$ \Delta B _{\text{bound}}^1 = \begin{bmatrix} 0 \\ 0 \\ 0 \\ 11.6233 \end{bmatrix}$
Degree-3	Moderate failure bound	$ \Delta A _{\text{bound}}^2 = \begin{bmatrix} 0 & 0 & 0 & 0 \\ 0 & 70.423 & 0 & 0 \\ 0 & 0.22 \times 10^{10} & 3.5978 \times 10^2 & 3.5266 \times 10^{13} \\ 0 & 0 & 0 & 0 \end{bmatrix}$	$ \Delta B _{\text{bound}}^2 = \begin{bmatrix} 0 \\ 0 \\ 0 \\ 23.2466 \end{bmatrix}$

Remark 3. Since the proposed FTC strategy in this paper focused on gradual faults under certain range, and obtained the optimized PFTC control gain by using convex optimization technique, for the system with minor fault conditions (performance status (b)), or for more severe moderate fault conditions (performance status (c)) when the FTC effect can have requested system tracking performance, it is applicable. Unfortunately, for the system with major fault conditions (performance status (d)), the solved control gain would have limited effect; therefore, another AFTC strategy (switching to Mode-2 quickly and smoothly) should be studied in the future work, as the situation is no longer discussed in this paper.

The previous analysis of pole distribution as a function of the fault severity leads to a conclusion that even gradual faults can affect the pole distribution. The system response performance is discussed in the following section, and the rationale for the necessity to develop PFTC strategy under gradual fault conditions is presented.

5.2. Analysis of Gradual Fault Effects in Time-Domain

The effects of gradual faults of different severity levels and different command inputs are presented and discussed in this section. The system response to a square-wave input and a sine-wave are studied, and the results, displacement response and the tracking error, are presented (see Figure 9). The minor fault upper bounds matrices are set as stated in Table 6. The system response to the square-wave input and the response to the compound sine-wave input indicate that, under the minor fault conditions, the tracking performance decreases slightly and the tracking errors increase compared with the system response under normal operating conditions.

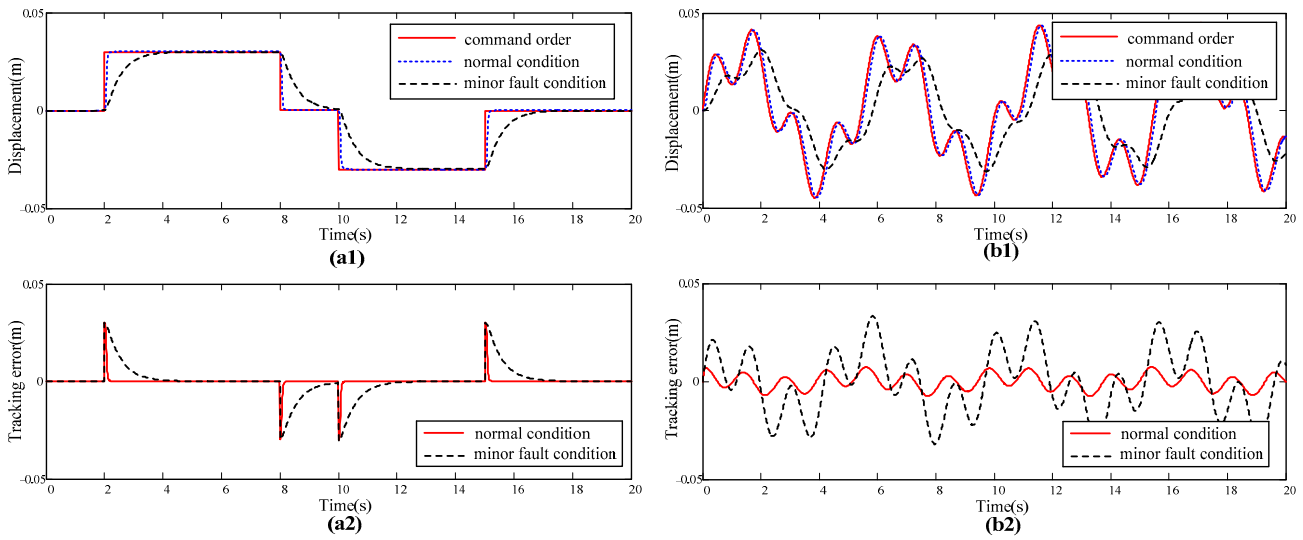


Figure 9. Tracking responses under minor fault conditions: (a1,a2) Displacement response to square-wave input; (b1,b2) Displacement response to compound sine-wave input.

The system response is also analyzed under the condition of a moderate fault (see Figure 10), where the upper bound matrices are set as shown in Table 6. The same square-wave input and the compound sine-wave are used to analyze the system response. The main difference between the system responses under different fault levels is that under moderate fault conditions, tracking performance decreases faster while tracking errors increase to a higher degree compared with those under normal conditions.

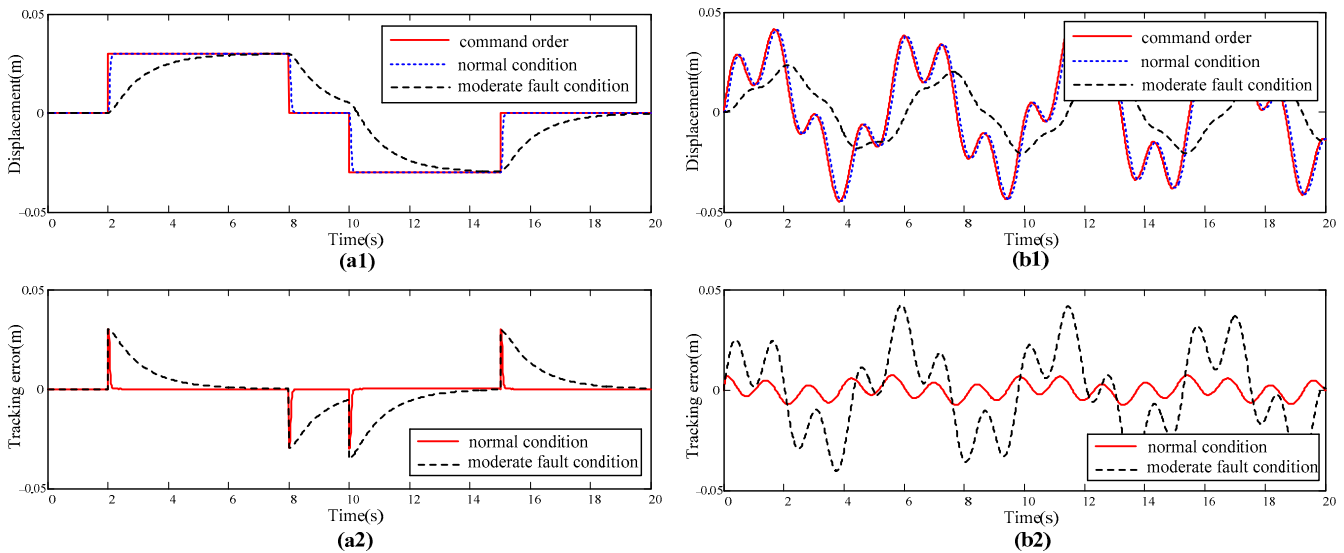


Figure 10. Tracking responses under moderate fault conditions: (a1,a2) Displacement response to square-wave input; (b1,b2) Displacement response to compound sine-wave input.

To calculate the quantized value under integrated fault conditions, the start and end times are set as $t_1 = 0$ and $t_2 = 20$, all evaluation results are shown in Table 7. It can be seen that with the fault degree increasing, the quantized value $e_{perf}(t)$ also shows an increasing trend. Under minor fault conditions, the value increases 102% compared with normal state by calculation, while under moderate fault conditions it increases 134%. Since gradual faults have apparent impacts on the system performance and it is difficult to detect the specific fault mode, the NT-DRAS cannot work as effectively for a system under the fault

conditions as under the normal conditions. Hence, it can be concluded that an appropriate FTC strategy should be developed and implemented.

Table 7. System performance evaluation values under integrated fault conditions without FTC.

Fault Conditions	$e_{\text{perf}}(t)$	$\bar{e}_{\text{perf}}(t)$	$e_{\text{perf-max}}$
Normal	0.4307	0.0000771	0.03
Minor fault	0.8721	0.0003205	0.03
Moderate fault	1.0098	0.0004153	0.03

Square-wave signal is used to evaluate the tracking performance here.

5.3. Simulation Results Using FTC Strategies

In this section, different FTC strategies are presented and respective simulation results are used to analyze the system response. The system model with moderate failure is used in the following analysis, where the corresponding matrices are presented in Table 6. Different FTC methods are used to form a closed-loop system and compare the control effects. Since the gradual faults are considered in the NT-DRAS, the FTC target should be maintaining the system robust performance under gradual fault conditions. Meanwhile, the FTC controller should be with a fixed structure as well as an efficient and effective control gain, which can not only save the control resources but also ensure the system reliability during the FTC process. Based on the above consideration, two fault-tolerant control methods analyzed in this section are guaranteed cost control (GCC) method [33] and CO-FTC method proposed in this paper.

Remark 4. GCC method is robust control design method for system with considered uncertainty [33]. The method is suitable for the following uncertain system:

$$\dot{x}(t) = (A + \Delta A)x(t) + (B + \Delta B)u(t) \tag{26}$$

A cost function in the following form

$$J = \int_0^t (x^T(\tau)Qx(\tau) + u(\tau)^TRu(\tau))d\tau \tag{27}$$

was defined to deal with the uncertain matrices, $[\Delta A \ \Delta B] = DF[E_1 \ E_2]$, where matrices D and E describe the structure information. The corresponding control gain form is given as an LMI condition (see (19)), where X and W are positive matrices, then for a given positive scalar ϵ , and if the LMI holds, then, the state feedback guaranteed cost control law can be designed as $K = WX^{-1}$ where the cost has upper bound $J \leq x_0^{-1}X^{-1}x_0$.

From Remark 4, it is shown that GCC is a fault-tolerant control gain design method based on state feedback, where weighting matrices Q and R are chosen to decrease defined cost functional. As opposed to the GCC, the proposed OP-FTC uses not only state feedback but also the output error integration feedback to design the control law. In order to remove the system uncertainty, new conditions, based on convex analysis, are deduced and the control gain matrix determined from the corresponding LMIs. The comparison between the two methods applied to the system under the same moderate failure is shown in Figure 11.

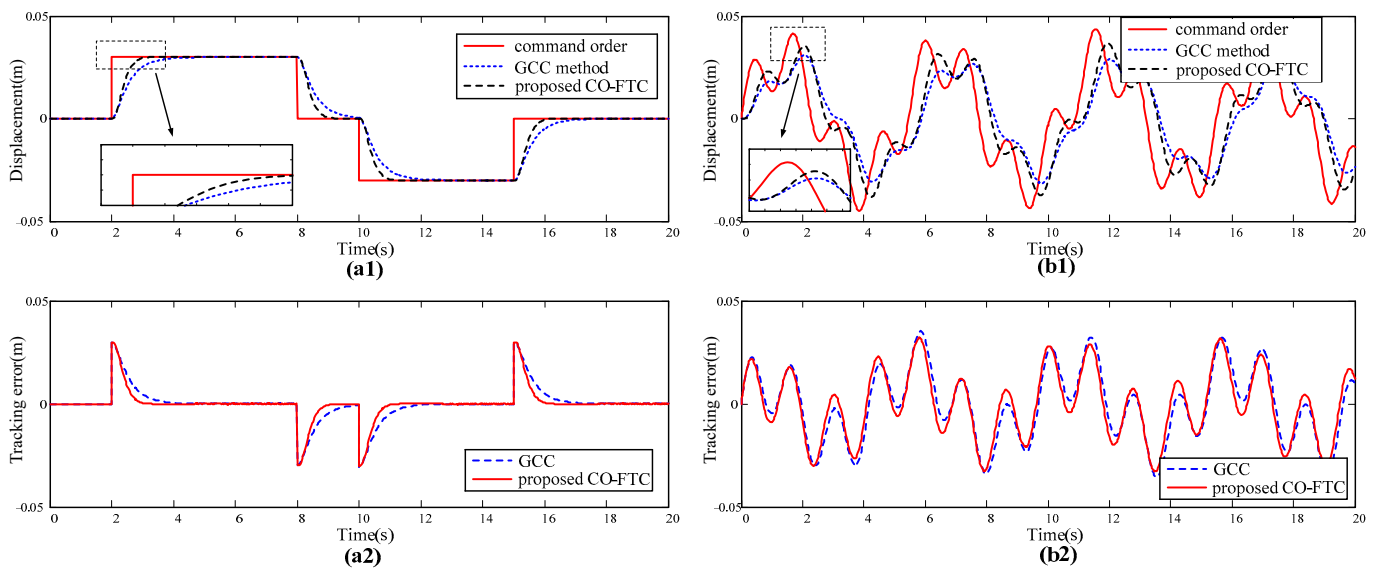


Figure 11. Tracking responses under moderate fault conditions using PFTC approaches: (a1,a2) Displacement response with square-wave input; (b1,b2) Displacement response to compound sine-wave input.

The system response to a square-wave and to a compound sine-wave input is compared for the cases when the GCC method and the proposed OP-FTC method are applied (see Figure 11). The results indicate that both GCC and OP-FTC methods can improve the tracking performance of the system with moderate fault with respect to both the square-wave and the compound sine-wave inputs. The Figure 11(a1,b1) show the local details of tracking performance for both control methods. The simulation results indicate that the system under moderate fault and with the proposed CO-FTC control method can track the command input better than when using the GCC control method: To track the square-wave reference signal, the rising time using the proposed CO-FTC control method is about 1 s while the rising time using the GCC control method is about 2 s (see Figure 11(a1)). Meanwhile, the tracking error former control method converges faster than the error using the latter control method (see Figure 11(a2)). To track a compound sine-wave reference signal, using the former control method, the tracking performance has less time lag and smaller peak error compared with it using the later control method (see Figure 11(b1,b2)). The tracking performance under different fault conditions by using both GCC and CO-FTC are quantized and shown in Table 8. Under minor fault conditions, the quantized tracking performance error has 26.25% reduction by using GCC method, while it has 35.09% reduction by using CO-FTC method. Under moderate fault conditions, the quantized tracking performance error has 34.56% reduction by using GCC method, while it has 43.18% reduction by using CO-FTC method. This result indicates that the proposed CO-FTC method has better fault tolerant effectiveness compared to GCC control method, and the compared advantage is increasingly obvious with the gradual faults increasing.

Table 8. System performance evaluation values under integrated fault conditions by using FTC.

Fault Conditions	$e_{perf}(t)$			$\bar{e}_{perf}(t)$			$e_{perf-max}$
Item	Original	GCC	CO-FTC	Original	GCC	CO-FTC	
Normal	0.4307	\	\	0.0000771	\	\	0.03
Minor fault	0.8721	0.6432	0.5661	0.0003205	0.0002274	0.0001405	0.03
Moderate fault	1.0098	0.6608	0.5738	0.0004153	0.0002382	0.0001445	0.03

Square-wave signal is used to evaluate the tracking performance here.

6. Conclusions

In this paper, a novel CO-FTC strategy has been proposed for NT-DRAS subject to gradual faults, where the gradual faults are described as the parameter drift with upper bound value. In applying the pole analysis method and evaluating the performance response in the time domain, the effectiveness of FTC for NT-DRAS with gradual faults is demonstrated. Since gradual faults are difficult to detect in a timely manner, NT-DRAS with gradual faults is modeled with uncertainty, and a CO-FTC strategy is proposed to design a fixed controller to improve the system performance. The control gain matrix of the fixed controller was optimized by LMI technique to realize the optimal pole placement. The proposed CO-FTC proves to be effective when dealing with gradual faults such as leakage and flow changes, which are difficult to detect in NT-DRAS. However, once these types of faults increase to a higher degree of severity, fault detection and diagnosis (FDD) information can be obtained through appropriate AFTC strategies, which are more efficient in dealing with serious fault conditions.

Author Contributions: Conceptualization, J.W.; methodology, C.S.; validation, F.Z., C.S. and W.L.; formal analysis, J.W.; investigation, W.L.; resources, W.L.; data curation, F.Z.; writing—original draft preparation, J.W.; writing—review and editing, D.L.; visualization, J.H.; supervision, J.H.; project administration, J.H.; funding acquisition, J.W. All authors have read and agreed to the published version of the manuscript.

Funding: This work was supported by the National Natural Science Foundation of China (Grant No. 52105049, 52175038 and 52205046).

Institutional Review Board Statement: Not applicable.

Informed Consent Statement: Not applicable.

Data Availability Statement: The data presented in this study are available on request from the corresponding author. The data are not publicly available due to privacy.

Conflicts of Interest: The authors declare no conflict of interest.

Appendix A

If $A_L + B_L K_x$ is Hurwitz stable, which means all the eigenvalues of the matrix have negative real parts $\text{Re}\lambda_i(A_L + B_L K_x) < 0$. The congruence of the matrix $A_L + B_L K_x$ by transformation matrix T_1 does not change the eigenvalues

$$T_1^{-1}(A_L + B_L K_x)T_1 = \Lambda_L + (\hat{B}_L \hat{K}_x) \quad (\text{A1})$$

where T_1^{-1} is the inverse matrix of T_1 . Since $\Lambda_L + (\hat{B}_L \hat{K}_x)$ is the diagonal form of the matrix $A_L + B_L K_x$, it leads to $\text{Re}\lambda_i(\Lambda_L + (\hat{B}_L \hat{K}_x)) < 0$. Following the concrete forms of matrices A_L and B_L in Lemma 1, another form of the real parts of these eigenvalues can be rewritten as

$$\text{Re}[\lambda_i(A) \pm \lambda_i(|\Delta A|_{\text{bound}}) + \lambda_i(B \hat{K}_x) \pm \lambda_i(|\Delta B|_{\text{bound}} \hat{K}_x)] < 0 \quad (\text{A2})$$

According to Assumption 1, even if the maximum value condition of the above formula is chosen, it still holds that

$$\begin{aligned} & \max \text{Re}[\lambda_i(A) \pm \lambda_i(|\Delta A|_{\text{bound}}) + \lambda_i(B \hat{K}_x) \pm \lambda_i(|\Delta B|_{\text{bound}} \hat{K}_x)] \\ & = -|\text{Re}\lambda_i(A)| + |\text{Re}\lambda_i(|\Delta A|_{\text{bound}})| - |\text{Re}\lambda_i(B \hat{K}_x)| + |\text{Re}\lambda_i(|\Delta B|_{\text{bound}} \hat{K}_x)| < 0 \end{aligned} \quad (\text{A3})$$

Similarly, to feedback the pair matrix $(A + \Delta A \quad B + \Delta B)$ with K_x and then congruence it with another transformation matrix T_2 , then the eigenvalues of the transformation result can be obtained as

$$\begin{aligned} & \text{Re}\lambda_i(A + \Delta A + (B + \Delta B)K_x) \\ & = \text{Re}[\lambda_i(A) + \rho_A \times \lambda_i(|\Delta A|_{\text{bound}}) + \lambda_i(BK_x) + \rho_B \times \lambda_i(|\Delta B|_{\text{bound}} \hat{K}_x)] \end{aligned} \quad (\text{A4})$$

where ρ_A and ρ_B are random variables as time independent factors(see Section 3.1). Since the two variables $\rho_A \in [-1, +1]$ and $\rho_B \in [-1, +1]$, the following inequality can be obtained as

$$\begin{aligned} & \text{Re}[\lambda_i(A) + \rho_A \times \lambda_i(|\Delta A|_{\text{bound}}) + \lambda_i(BK_x) + \rho_B \times \lambda_i(|\Delta B|_{\text{bound}}\hat{K}_x)] \\ & < -|\text{Re}\lambda_i(A)| + |\text{Re}\lambda_i(|\Delta A|_{\text{bound}})| - |\text{Re}\lambda_i(B\hat{K}_x)| + |\text{Re}\lambda_i(|\Delta B|_{\text{bound}}\hat{K}_x)| \end{aligned} \tag{A5}$$

From the Formulas (A3)–(A5), it can be deduced that

$$\begin{aligned} & \text{Re}\lambda_i(A + \Delta A + (B + \Delta B)K_x) \\ & < \max\text{Re}[\lambda_i(A) \pm \lambda_i(|\Delta A|_{\text{bound}}) + \lambda_i(B\hat{K}_x) \pm \lambda_i(|\Delta B|_{\text{bound}}\hat{K}_x)] \end{aligned} \tag{A6}$$

Therefore, the following inequality is obtained to illustrate the conclusion, which is proven as follows:

$$\text{Re}\lambda_i(A + \Delta A + (B + \Delta B)K_x) \leq \text{Re}\lambda_i(\Lambda_L + (\hat{B}_L\hat{K}_x)) < 0 \tag{A7}$$

This is the end of proof for Lemma 1.

Appendix B

According to [23,27], the sufficient condition for the existence of the fault-tolerant controller with the constraints of linear quadratic (LQ) performance can be restated as

$$(A_{\text{aug}} + B_{\text{aug}}K)^T P + P(A_{\text{aug}} + B_{\text{aug}}K) + Q + K^T R K + \left(\frac{1}{\gamma^2}\right) P G_{\text{aug}} G_{\text{aug}}^T P < 0 \tag{A8}$$

Using Lemma 3 and choosing $\psi = Q + K^T R K + \left(\frac{1}{\gamma^2}\right) P G_{\text{aug}} G_{\text{aug}}^T P$, $\zeta = P(A_{\text{aug}} + B_{\text{aug}}K)$, this sufficient condition can be transformed into the following form by using Lemma 4.

$$\begin{bmatrix} Q + K^T R K + \left(\frac{1}{\gamma^2}\right) P G_{\text{aug}} G_{\text{aug}}^T P + P - \begin{pmatrix} - & -^T \\ S & S \end{pmatrix} & S^T + (A_{\text{aug}} + B_{\text{aug}}K)^T P \\ S + P(A_{\text{aug}} + B_{\text{aug}}K) & -P \end{bmatrix} < 0 \tag{A9}$$

By a congruence transformation matrix $\begin{bmatrix} V & 0 \\ 0 & X \end{bmatrix}$ with $V = S^{-1}$ and $X = P^{-1}$, the following form can be further deduced.

$$\begin{bmatrix} V^T Q V + V^T K^T R K V + \left(\frac{1}{\gamma^2}\right) V^T P G_{\text{aug}} G_{\text{aug}}^T P V + V^T P V - (V+V^T) & X + V^T (A_{\text{aug}} + B_{\text{aug}}K)^T \\ (A_{\text{aug}} + B_{\text{aug}}K) V + X & -X \end{bmatrix} < 0 \tag{A10}$$

By multiple applications of Lemma 4 and by defining $N = KV$ and $M = PV$, the deduced form can be transformed into the final form as follows:

$$\begin{bmatrix} -(V+V^T) & X+V^T A_{\text{aug}}^T + N^T B_{\text{aug}}^T & V^T & M^T G_{\text{aug}}^T & V^T & N^T \\ * & -X & 0 & 0 & 0 & 0 \\ * & * & -X & 0 & 0 & 0 \\ * & * & * & -\gamma^2 I & 0 & 0 \\ * & * & * & * & -Q^{-1} & 0 \\ * & * & * & * & * & -R^{-1} \end{bmatrix} < 0 \tag{A11}$$

Since the matrices A_{aug} and B_{aug} have uncertain modules A_F and B_F respectively, therefore, the final deduced LMI form cannot be solved. Applying Lemma 1, which is intended to remove uncertainty based on the convex analysis and proof, the uncertain

modules can be replaced with their boundary forms A_L and B_L . Consequently, the solvable LMI forms can be obtained as follows:

$$\begin{bmatrix} -(V+V^T) & X+V^T A_L^T+N^T B_L^T & V^T & M^T G_{aug}^T & V^T & N^T \\ * & -X & 0 & 0 & 0 & 0 \\ * & * & -X & 0 & 0 & 0 \\ * & * & * & -\gamma^2 I & 0 & 0 \\ * & * & * & * & -Q^{-1} & 0 \\ * & * & * & * & * & -R^{-1} \end{bmatrix} < 0 \tag{A12}$$

Since the control law form (see Equation (21)) is chosen to stabilize the augmented system (see Equation (20)), using the treatment method similar to the one used in [27] it can be substituted into the LQ cost function form and result in:

$$\begin{aligned} J &= \int_0^t x_{aug}^T(\tau) (Q + K^T R K) x_{aug}(\tau) d\tau \\ &< -\int_0^t x_{aug}^T(\tau) \left[(A_{aug} + B_{aug} K)^T P + P (A_{aug} + B_{aug} K) + \left(\frac{1}{\gamma^2}\right) P G_{aug} G_{aug}^T P \right] x_{aug}(\tau) d\tau \\ &= -\int_0^t \left[(\dot{x}_{aug}(\tau) - G_{aug} w_{aug}(\tau))^T P x_{aug}(\tau) + x_{aug}^T(\tau) P (\dot{x}_{aug}(\tau) - G_{aug} w_{aug}(\tau)) \right. \\ &\quad \left. + x_{aug}^T(\tau) \left(\frac{1}{\gamma^2}\right) P G_{aug} G_{aug}^T P x_{aug}(\tau) \right] d\tau \\ &\leq -\int_0^t d \left(x_{aug}^T(\tau) P x_{aug}(\tau) \right) + \gamma^2 \int_0^t w_{aug}^T(\tau) w_{aug}(\tau) d\tau \\ &= x_{aug}^T(0) P x_{aug}(0) + \gamma^2 \int_0^t w_{aug}^T(\tau) w_{aug}(\tau) d\tau \end{aligned} \tag{A13}$$

This is the end of proof for Theorem 1.

References

1. Yongling, F.; Yao, P. Design and working mode analysis of dissimilar redundant actuator system. *J. Beijing Univ. Aeronaut. Astronaut.* **2012**, *38*, 432–437.
2. Zhang, Y.; Zhang, C.; Wang, S.; Chen, R.; Tomovic, M.M. Performance Degradation Based on Importance Change and Application in Dissimilar Redundancy Actuation System. *Mathematics* **2022**, *10*, 843. [CrossRef]
3. Wang, S.; Cui, X.; Shi, J.; Tomovic, M.M.; Jiao, Z. Modeling of reliability and performance assessment of a dissimilar redundancy actuation system with failure monitoring. *Chin. J. Aeronaut.* **2016**, *29*, 799–813. [CrossRef]
4. Yu, M.; Meng, J.; Zhu, R.; Jiang, W.; Shen, Q. Sensor fault diagnosis for uncertain dissimilar redundant actuation system of more electric aircraft via bond graph and improved principal component analysis. *Meas. Sci. Technol.* **2022**, *34*, 015120. [CrossRef]
5. Wang, J.; Wang, S.; Wang, X.; Shi, C.; Tomovic, M.M. Active fault tolerant control for vertical tail damaged vehicle with dissimilar redundant actuation system. *Chin. J. Aeronaut.* **2016**, *29*, 1313–1325. [CrossRef]
6. Zhang, Y.; Jiang, J. Bibliographical review on reconfigurable fault-tolerant control systems. *Annu. Rev. Control* **2008**, *32*, 229–252. [CrossRef]
7. Niemann, H.; Stoustrup, J. Passive fault tolerant control of a double inverted pendulum—A case study. *Control Eng. Pract.* **2005**, *13*, 1047–1059. [CrossRef]
8. Castaldi, P.; Mimmo, N.; Simani, S. Differential geometry based active fault tolerant control for vehicle. *Control Eng. Pract.* **2014**, *32*, 227–235. [CrossRef]
9. Goupil, P. AIRBUS state of the art and practices on FDI and FTC in flight control system. *Control Eng. Pract.* **2011**, *19*, 524–539. [CrossRef]
10. Fekih, A. Fault-tolerant flight control design for effective and reliable vehicle systems. *J. Control Decis.* **2014**, *1*, 299–316. [CrossRef]
11. Tao, G. Direct adaptive actuator failure compensation control: A tutorial. *J. Control Decis.* **2014**, *1*, 75–101. [CrossRef]
12. Chen, J.; Zhang, W.; Cao, Y.-Y. Robust reliable feedback controller design against actuator faults for linear parameter-varying systems in finite-frequency domain. *IET Control Theory Appl.* **2015**, *9*, 1595–1607. [CrossRef]
13. Chen, M.; Liu, X.; Wang, H. Adaptive robust fault-tolerant control for nonlinear systems with prescribed performance. *Nonlinear Dyn.* **2015**, *81*, 1727–1739. [CrossRef]
14. Tao, Y.; Shen, D.; Fang, M.; Wang, Y. Reliable H_∞ control of discrete-time systems against random intermittent faults. *Int. J. Syst. Sci.* **2016**, *47*, 2290–2301. [CrossRef]
15. Zhang, W.; Lou, W.; Tong, S. Fault-tolerant control against actuator faults for a class of ts fuzzy discrete-time interconnected systems. *ICIC Express Lett. Part B Appl. Int. J. Res. Surv.* **2015**, *6*, 717–722.
16. Oliver, N. *Nonlinear System Identification: From Classical Approaches to Neural Networks and Fuzzy Models*; Springer: Berlin/Heidelberg, Germany, 2001; Volume 11, pp. 294–296.
17. Xiang, Y.; Youmin, Z. Design of passive fault-tolerant flight controller against actuator failures. *Chin. J. Aeronaut.* **2015**, *28*, 180–190.

18. Zhou, S.; Zheng, W.X. Robust H_∞ control of delayed singular systems with linear fractional parametric uncertainties. *J. Frankl. Inst.* **2009**, *346*, 147–158. [[CrossRef](#)]
19. Wang, W.; Nguang, S.K.; Zhong, S.; Liu, F. Robust stability analysis of stochastic delayed genetic regulatory networks with polytopic uncertainties and linear fractional parametric uncertainties. *Commun. Nonlinear Sci. Numer. Simul.* **2014**, *19*, 1569–1581. [[CrossRef](#)]
20. Li, Y.-X.; Yang, G.-H. Robust fuzzy adaptive fault-tolerant control for a class of nonlinear systems with mismatched uncertainties and actuator faults. *Nonlinear Dyn.* **2015**, *81*, 395–409. [[CrossRef](#)]
21. Chesi, G. LMI conditions for time-varying uncertain systems can be non-conservative. *Automatica* **2011**, *47*, 621–624. [[CrossRef](#)]
22. Kheloufi, H.; Zemouche, A.; Bedouhene, F.; Boutayeb, M. On LMI conditions to design observer-based controllers for linear systems with parameter uncertainties. *Automatica* **2013**, *49*, 3700–3704. [[CrossRef](#)]
23. Liao, F.; Wang, J.L.; Yang, G.-H. Reliable robust flight tracking control: An LMI approach. *IEEE Trans. Control Syst. Technol.* **2002**, *10*, 76–89. [[CrossRef](#)]
24. Shi, C.; Wang, S.; Wang, X.; Wang, J.; Tomovic, M.M. Active fault-tolerant control of dissimilar redundant actuation system based on performance degradation reference models. *J. Frankl. Inst.* **2017**, *354*, 1087–1108. [[CrossRef](#)]
25. Shi, C.; Wang, X.; Wang, S.; Wang, J.; Tomovic, M.M. Adaptive decoupling synchronous control of dissimilar redundant actuation system for large civil vehicle. *Aerosp. Sci. Technol.* **2015**, *47*, 114–124. [[CrossRef](#)]
26. Huang, Y.; Sun, C.; Qian, C. Linear parameter varying switching attitude tracking control for a near space hypersonic vehicle via multiple Lyapunov functions. *Asian J. Control* **2015**, *17*, 523–534. [[CrossRef](#)]
27. Yu, X.; Jiang, J. Hybrid fault-tolerant flight control system design against partial actuator failures. *IEEE Trans. Control Syst. Technol.* **2012**, *20*, 871–886. [[CrossRef](#)]
28. Tong, S.; Sui, S.; Li, Y. Fuzzy adaptive output feedback control of MIMO nonlinear systems with partial tracking errors constrained. *IEEE Trans. Fuzzy Syst.* **2015**, *23*, 729–742. [[CrossRef](#)]
29. Xu, Y.; Shaocheng, T.; Yongming, L. Adaptive fuzzy fault-tolerant control of static var compensator based on dynamic surface control technique. *Nonlinear Dyn.* **2013**, *73*, 2013–2023. [[CrossRef](#)]
30. Sakthivel, R.; Sundareswari, K.; Mathiyalagan, K.; Arunkumar, A.; Anthoni, S.M. Robust Reliable H_∞ Control for Discrete-Time Systems with Actuator Delays. *Asian J. Control* **2015**, *17*, 2133–2142. [[CrossRef](#)]
31. Apkarian, P. Continuous-time analysis and H_2 multi-channel synthesis with enhanced LMI characterizations. *IEEE Trans. Automat. Contr.* **2001**, *46*, 1941–1946. [[CrossRef](#)]
32. Zhang, F. *The Schur Complement and Its Applications*; Springer Science & Business Media: Berlin, Germany, 2006; Volume 4.
33. Li, X.; Liu, H.H. A passive fault tolerant flight control for maximum allowable vertical tail damaged vehicle. *J. Dyn. Syst. Meas. Control* **2012**, *134*, 031006. [[CrossRef](#)]

Disclaimer/Publisher’s Note: The statements, opinions and data contained in all publications are solely those of the individual author(s) and contributor(s) and not of MDPI and/or the editor(s). MDPI and/or the editor(s) disclaim responsibility for any injury to people or property resulting from any ideas, methods, instructions or products referred to in the content.